

Article

Tracking Cerebral Microvascular and Metabolic Parameters during Cardiac Arrest and Cardiopulmonary Resuscitation

Nima Khalifehsoltani ^{1,*}, Olivia Rennie ², Rohit Mohindra ^{3,4}, Steve Lin ⁵ and Vladislav Toronov ^{1,*}¹ Department of Physics, Toronto Metropolitan University, 350 Victoria Street, Toronto, ON M5B 2K3, Canada² Temerty Faculty of Medicine, University of Toronto, 1 King's College Cir., Toronto, ON M5S 1A8, Canada; olivia.rennie@mail.utoronto.ca³ Schwartz Reisman Emergency Institute, Toronto, ON M5G 1X5, Canada⁴ North York General Hospital, 4001 Leslie St., Toronto, ON M2K 1E1, Canada⁵ Keenan Research Centre, Li Ka Shing Knowledge Institute, St. Michael's Hospital, 30 Bond St., Toronto, ON M5B 1W8, Canada

* Correspondence: nima.khalifehsoltani@torontomu.ca (N.K.); toronov@torontomu.ca (V.T.)

Abstract: Hemodynamic models provide a mathematical representation and computational framework that describe the changes in blood flow, blood volume, and oxygenation levels that occur in response to neural activity and systemic changes, while near-infrared spectroscopy (NIRS) measures deoxyhemoglobin, oxyhemoglobin, and other chromophores to analyze cerebral hemodynamics and metabolism. In this study, we apply a dynamic hemometabolic model to NIRS data acquired during cardiac arrest and cardiopulmonary resuscitation (CPR) in pigs. Our goals were to test the model's ability to accurately describe the observed phenomena, to gain an understanding of the intricate behavior of cerebral microvasculature, and to compare the obtained parameters with known values. By employing the inverse of the hemometabolic model, we measured a range of significant physiological parameters, such as the rate of oxygen diffusion from blood to tissue, the arteriole and venule volume fractions, and the Fåhræus factor. Statistical analysis uncovered significant differences in the baseline and post-cardiac arrest values of some of the parameters.



Citation: Khalifehsoltani, N.; Rennie, O.; Mohindra, R.; Lin, S.; Toronov, V. Tracking Cerebral Microvascular and Metabolic Parameters during Cardiac Arrest and Cardiopulmonary Resuscitation. *Appl. Sci.* **2023**, *13*, 12303. <https://doi.org/10.3390/app132212303>

Academic Editor: Herbert Schneckenburger

Received: 26 September 2023

Revised: 1 November 2023

Accepted: 9 November 2023

Published: 14 November 2023



Copyright: © 2023 by the authors. Licensee MDPI, Basel, Switzerland. This article is an open access article distributed under the terms and conditions of the Creative Commons Attribution (CC BY) license (<https://creativecommons.org/licenses/by/4.0/>).

Keywords: near-infrared spectroscopy; NIRS; brain; neuronal activity; cardiac arrest; hemodynamic model; cardiopulmonary resuscitation; CPR; hyperspectral near-infrared spectroscopy; microvasculature; hemodynamic model; hemometabolic model; laser Doppler flowmetry; diffuse correlation spectroscopy

1. Introduction

Out-of-hospital cardiac arrest (CA) is a major public health challenge, with an average global incidence among adults of 55 CAs per 100,000 person-years [1]. Among CA patients who receive cardiopulmonary resuscitation (CPR), the survival rates are as follows: 29.7% upon achieving return of spontaneous circulation (ROSC), 22.0% upon hospital admission, and 8.8% upon hospital discharge. The pooled 1-month survival rate is 10.7% and the 1-year survival rate is 7.7% [1]. Monitoring the cerebral perfusion and metabolic parameters such as cerebral tissue oxygen saturation, cerebral blood volume (CBV), cerebral blood flow (CBF), cerebral metabolic rate of oxygen (CMRO₂), and mitochondrial oxygen metabolism is crucial for improving survival and recovery rates. Near-infrared spectroscopy (NIRS) measures changes in oxyhemoglobin (HbO₂) and deoxyhemoglobin (HHb), reflecting alterations in CBV, CBF, and CMRO₂ [2]. However, current NIRS techniques are limited in their sensitivity to the brain [2], cytochrome C oxidase [3], and CMRO₂ [4], necessitating further improvements. Another vital aspect in the realm of NIRS is the interpretation of its recordings with respect to physiological dynamics. In this regard, hemodynamic models have been introduced to establish relationships between physiological perturbations and measured quantities. Hemodynamic models have advanced significantly, notably with

the integration of imaging techniques such as NIRS and functional magnetic resonance imaging (fMRI). In this study, a novel coherent hemodynamic spectroscopy (CHS) model [5] is applied to invasively obtained cerebral hyperspectral NIRS (hNIRS) data obtained from pigs during induced CA to assess changes in CBV, CBF, and CMRO₂ during CA and CPR, providing valuable insights into the capturing of perturbations associated with CA and CPR. Several hemometabolic parameters were utilized to derive quantitative predictions from the model.

The CHS model [5] calculates blood oxygen saturations for both simple and complex vascular topologies, resulting in equations for the values of the average tissue oxyhemoglobin (HbO₂) and deoxyhemoglobin (HHb) concentrations over the arteriole, capillary, and venule compartments. For straightforward topologies, the assumption centers on a sequence of a single arteriole, followed by a capillary, and finally a venule. In more complex scenarios, various orders and additional components are considered. Dynamic equations governing oxygen saturation in all three components—arterioles, capillaries, and venules—generate the values used to compute changes in oxy- and deoxyhemoglobin over time.

Direct applications have been found for the CHS model in various studies related to cerebral hemodynamics and functional neuroimaging. Hiura et al. [6] utilized the CHS model to explore the relationships between cerebral oxygen metabolism and perfusion during exercise using NIRS. Blaney et al. [7] applied dual-slope imaging of cerebral hemodynamics with frequency-domain NIRS, incorporating the principles of the CHS model. Furthermore, the algorithm introduced by Blaney et al. [8] for determining significant coherence thresholds in time–frequency analyses was based on the CHS model's principles. These investigations collectively highlight the adaptability and significance of the CHS model in advancing our comprehension of brain physiology and its utility in functional neuroimaging [6–8]. The CHS model is a dynamic model that quantifies the temporal evolution of the concentration and oxygen saturation of hemoglobin in tissue, as determined by time-varying hemodynamic and metabolic parameters: blood volume, flow velocity, and oxygen consumption [9]. Initially, the linear version of the model [9] was tested in the context of a study on cardiac arrest in pigs; however, this yielded no acceptable outcomes, aligning with the authors' assertion that the linear model is effective for perturbations smaller than 10% of the baseline in capillary blood flow velocity. Subsequently, our investigation turned to the non-linear version of this model [5]. A distinctive characteristic of the non-linear version is the non-linear dependence on the flow velocity in both capillary and venous compartments, a feature not present in the linear version.

Another hemometabolic model presented by Banaji et al. [10] has been widely embraced in diverse inquiries concerning cerebral circulation, metabolism, and changes in NIRS signals. Russell-Buckland and Tachtsidis [11] employed this model to simulate the influence of hypothermia on cerebral blood flow and metabolism. Russell-Buckland et al. [12] introduced a Bayesian framework for the examination of systems biology models of the brain which encompasses the referenced model. Siddiqui et al. [13] employed the model for the non-invasive assessment of markers of infant brain function, while Caldwell et al. [14] employed it to model extracerebral contamination and systemic factors when analyzing fNIRS data. Hapuarachchi et al. [15] simulated preterm neonatal brain metabolism during neuronal activation, and Caldwell et al. [16] applied the model to investigate blood flow and metabolism during neonatal hypoxic–ischemic events. These studies collectively underscore the versatility of the model in investigating brain physiology and the implications this has for neonatal care, systems biology analysis, and the enhancement of NIRS-based measurements [10–16]. In a subsequent phase of our research, we plan to investigate the model proposed in [10] for the study of cardiac arrest in pigs. However, the model proposed in [10] contains 27 equations for nearly 50 parameters and variables, making it considerably more complex than the CHS model [5]. Therefore, for our initial investigation of the applicability of dynamic hemometabolic models to microvascular cerebral changes during CA, we selected the CHS model.

2. Materials and Methods

2.1. Hemodynamic Model

The equations of the forward non-linear CHS model [5] are presented in the Appendix A. According to this model, the time dependent alterations in HbO₂ and HHb resulted from the changes in blood flow speed and blood volume. The dynamic inputs of the model were the total hemoglobin concentration measured using NIRS and the blood flow velocity index measured using laser Doppler flowmetry (see Figure 1a).

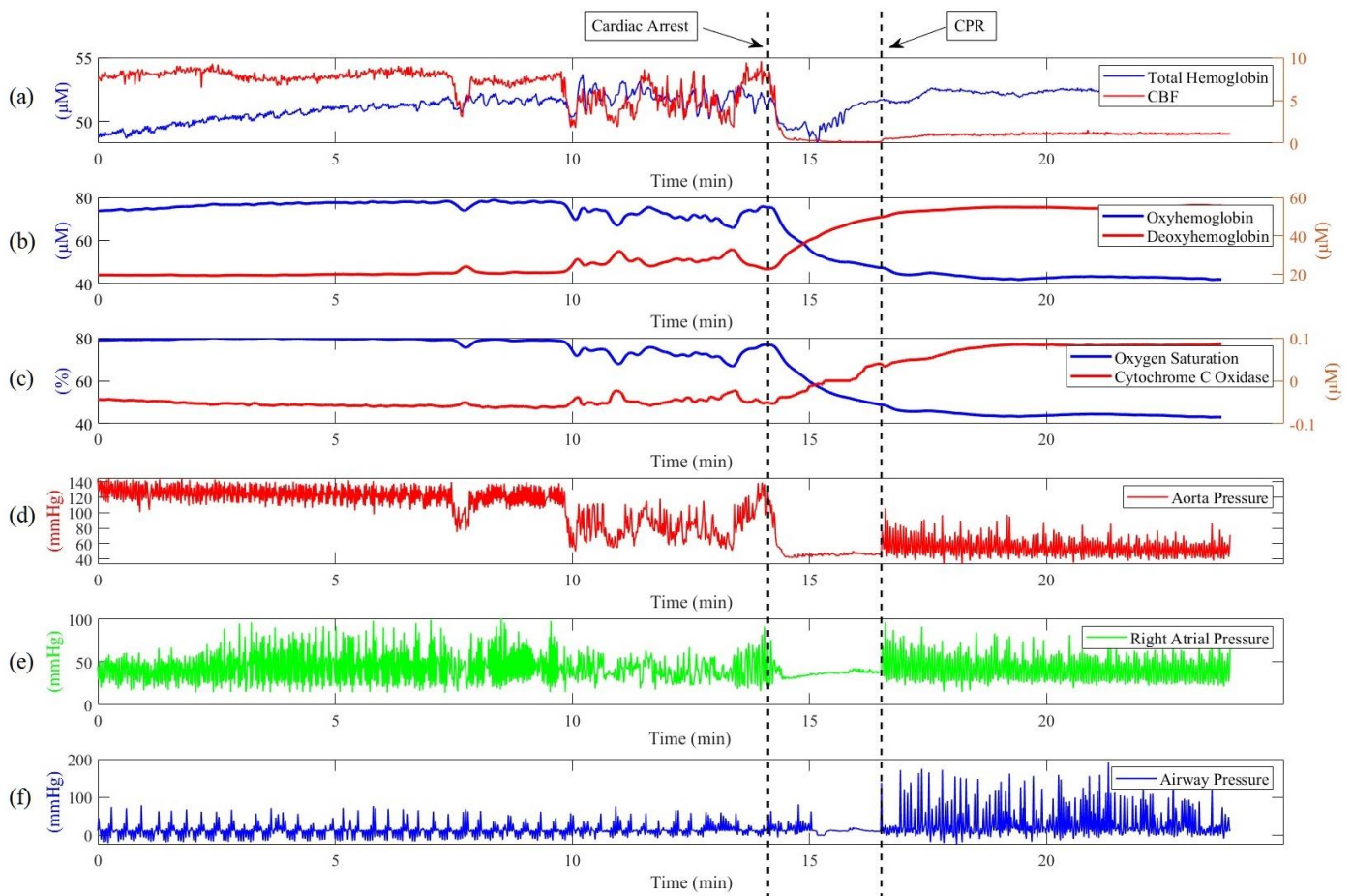


Figure 1. Changes in physiological data from a single experiment. The data include (a) total hemoglobin and cerebral blood flow velocity; (b) oxy- and deoxyhemoglobin; (c) oxygen saturation and cytochrome c oxidase; (d) aortic pressure; (e) right arterial pressure; and (f) airway pressure. The left vertical line shows the onset of VF, while the right vertical line shows the onset of CPR.

A number of hemometabolic parameters were used to derive the quantitative predictions of the model. These parameters included the average microvascular concentration of the total hemoglobin in the blood ($ctHb$), the rate constant of oxygen diffusion from blood to tissue (α_o), the effective combined length of the small arterioles and capillaries ($L^{(c)}$), the effective combined length of the venules ($L^{(v)}$), the capillary baseline blood volume ratio ($Fp^{(c)}$), the venule blood flow factor ($fc^{(v)}$), the Fåhræus factor ($F^{(c)}$) (the ratio of capillary to large vessel hematocrit), the baseline arterial oxygen saturation ($S_0^{(a)}$), the average capillary blood flow speed ($v^{(c)}$), and the volume fractions of the arterioles ($\varphi^{(a)}$), capillaries ($\varphi^{(c)}$), and venules ($\varphi^{(v)}$).

Each of these parameters addressed an important physiological characteristic. In particular, the rate constant of oxygen diffusion represents the speed at which oxygen molecules move through tissues, reflecting tissue oxygenation dynamics. The Fåhræus

factor explains changes in blood viscosity in relation to vessel diameter, which impact circulatory efficiency.

2.2. Cardiac Arrest and CPR Setup

Twenty-seven female pigs (female pigs were used to remove the bias of sex differences in susceptibility to ventricular fibrillation (VF) induction and because female pigs have a higher rate of ROSC) were fasted overnight and then sedated with ketamine (20 mg/kg intramuscularly, “Ketalean” by Bi-meda-MTC Animal Health, Cambridge, ON, Canada). Intubation and continuous isoflurane (1–3% mixed with oxygen) ensued. An Ohmeda ventilator (Ohio Medical Products, Madison, WI, USA) was used to support ventilation and the appropriate settings were used to stabilize pH, pCO₂, and pO₂ (pH 7.35–7.45, PCO₂ 35–45 mmHg, PO₂ > 100 mmHg). A normal saline (NS) infusion (2–4 mL/kg/h) was delivered via a cannulated ear vein to prevent hypovolemia. Electrocardiogram leads were attached and defibrillation patch electrodes (Zoll Medical, Inc., Chelmsford, MA, USA) were used to monitor cardiac status. Aortic pressure and right atrial pressure were recorded in real time via femoral artery catheters (Mikro-Tip Transducer; Millar Instruments, Houston, TX, USA). These parameters were used to monitor the condition of each animal at all times, and thus to determine the occurrence of CA (VF) [17].

All experimental procedures adhered to the Reporting of In Vivo Experiments guidelines [18]. Approval of the ethical protocols was granted by the Animal Care Committee of St. Michael’s Hospital (Toronto, ON, Canada), and all practices were in accordance with the *Guide for the Care and Usage of Laboratory Animals* provided by the U.S. National Institutes of Health (NIH Publication number 85–23, revised 1996).

2.3. Resuscitation Protocol

Before VF was initiated, the delivery of anesthetic gases to the animals was paused for 15 min, and they received propofol and fentanyl for sedation to minimize the anti-arrhythmic effects of the anesthetic gases. VF was induced for 2 min by burst pacing at a minimum of 300 Hz with a 10 mV pulse using a pacing catheter (AM-2200, ADInstruments, Castle Hill, Australia) which was introduced into the RV. Subsequent CPR involved closed chest compressions at a rate of 100 per minute using an automatic piston (LUCAS; Physio-Control Inc./Jolife AB, Lund, Sweden). Mechanical ventilation (Ohmeda ventilator, Ohio Medical Products, Gurnee, IL, USA) was maintained a rate of 10 breaths per minute with pure oxygen. An IV bolus dose of 0.015 mg/kg of epinephrine in NS at a concentration of 0.1 mg/mL followed by a 10 mL NS flush was given after 2 min of CPR and administered every 4 min for a total of three doses. In addition, an IV infusion of an equivalent volume of NS (as calculated above in the epinephrine infusion group) was started after 2 min of CPR and administered for a total of 12 min.

2.4. Cerebral hNIRS Setup and Measurements

Hyperspectral NIRS (hNIRS) enables the direct quantification of the absolute levels of HbO₂ and HHb in the tissue as well as the difference between the oxidized and reduced cytochrome C oxidase, Δ Cyt-ox [19,20]. To carry out the measurements of the cerebral variables, a custom-designed hNIRS system [19,20] was utilized. This involved positioning optodes on the dura mater and maintaining a spacing of 20 mm between them. This was achieved by drilling holes in the skull above the brain. With a differential path length factor of 5 and an interoptode distance of 20 mm, the average optical path length was estimated to be around 100 mm, with an approximate penetration depth of 16 mm [21–23]. This optical path length was chosen to mitigate the interference from the ~1 mm thick dura. The hNIRS system included a highly sensitive spectrometer (AvaSpec, Avantes, Lafayette, CO, USA) which recorded spectral data in the 700–1000 nm range. The hNIRS diffusion model analyzed the data to determine changes in cerebral HbO₂, HHb, and Cyt-ox [17]. The dynamic fluctuations in chromophore concentrations were deciphered using a multi-step data-fitting algorithm which was grounded in the analytical solution to

the diffusion equation for a semi-infinite medium and which integrated the extrapolated boundary condition. This algorithm yielded values for the tissue concentrations of HbO₂, HHb, and ΔCyt-ox [19,24]. The total hemoglobin and tissue oxygen saturation (tSO₂) was computed using the following equation:

$$\text{Total [Hb]} = [\text{HbO}_2] + [\text{HHb}] \quad \text{tSO}_2 = [\text{HbO}_2]/(\text{Total [Hb]}) \times 100\%$$

In addition to hNIRS, the cerebral blood flow velocity index (CBFV) was measured using a laser Doppler flowmeter (LDF) (Periflux; Perimed Inc., Ardmore, PA, USA), for which purpose a probe was placed on the dura mater via a hole drilled in the pig’s skull. Mean aortic pressure and right atrial pressure were also monitored during the experiments using catheters equipped with micro-manometer tips.

2.5. Analysis Methods

A data analysis was conducted using MATLAB R2023a (MathWorks, Natick, MA, USA). The calculations were executed over two distinct time periods. Initially, baseline hemodynamic variables were used to compute the parameters during a 10 min period before the onset of VF. The subsequent set of calculations focused on a 2 min timespan after VF was induced; this was selected as the timeframe for data analysis and parameter fitting processes. This 2 min interval following VF initiation represented a period during which no actions, such as CPR or drug administration, were undertaken.

To derive numerical results for the parameters, we employed the inverse of the non-linear version of the hemodynamic model using the MATLAB function *fmicon*. As inputs, the model employed total hemoglobin measurements from the hNIRS and CBFV indices captured using LDF. Its objective was to optimize the aforementioned hemometabolic parameters to ensure alignment between its outputs (HbO₂ and HHb) and the actual NIRS readings. The calculated parameters and their respective ranges were as follows: *ctHb* (2–2.6 mM), α_o (0.6–1.0 s⁻¹), $F^{(c)}$ (0.6–0.9), $S_0^{(a)}$ (0.8–0.99%), $Fp^{(c)}$ (0.2–0.8), $fc^{(v)}$ (0.1–0.7), $L^{(c)}$ (0.4–0.8 mm), $L^{(v)}$ (0.5–1.2 mm), $v^{(c)}$ (0.6–1.0 mm/s), and contributions to baseline blood volume from arterioles (0.001–0.05), capillaries (0.005–0.05), and venules (0.001–0.05) [9].

The cost function for the optimization was the reduced X² for the combined HbO₂ and HHb fits. We also calculated R² values for the combined HbO₂ and HHb fits. For the final calculation results, we only included the cases for which R² > 0.5.

We employed a paired *t*-test to compare the average parameter values during baseline and after CA.

3. Results

Figure 1 illustrates all the recorded data from the experiment for one of the pigs, while Figure 2 shows the HbO₂ and HHb traces measured using hNIRS, accompanied by the corresponding data acquired using the forward model of the non-linear version of the hemodynamic model for the same pig. Data from 27 pigs were collected and analyzed. Good R² values between 0.5 and 0.9 occurred for only 17 of the 27 datasets. The statistical numerical values for the parameters for these cases are presented in Table 1.

Table 1. Values of the fitted parameters averaged across 17 datasets for which R² > 0.5 (average R² of 0.719, average X² of 0.282) for the baseline conditions; reference value ranges obtained from the literature; average parameter baseline–post-CA differences; and corresponding *p*-values. Parameters with *p*-values less than 0.05 are shown in bold font.

Parameter/Analysis	Average ± Std (Baseline)	Reference Range	Average Difference	<i>p</i> -Value
$S_0^{(a)}$ (%)	0.906 ± 0.060	0.8–0.99	−0.004	0.855
<i>ctHb</i> (mM)	2.103 ± 0.097	2.0–2.6	+0.065	0.040

Table 1. Cont.

Parameter/Analysis	Average \pm Std (Baseline)	Reference Range	Average Difference	<i>p</i> -Value
$Fp^{(c)}$	0.559 ± 0.176	0.2–0.8	−0.021	0.760
$F^{(c)}$	0.705 ± 0.089	0.6–0.9	+0.073	0.008
α_o (s ^{−1})	0.762 ± 0.115	0.6–1.0	+0.035	0.399
$fc^{(v)}$	0.460 ± 0.102	0.1–0.7	+0.008	0.829
$L^{(c)}$ (mm)	0.553 ± 0.092	0.4–0.8	−0.041	0.368
$L^{(v)}$ (mm)	1.012 ± 0.028	0.5–1.2	−0.007	0.637
$v^{(c)}$ (mm/s)	0.819 ± 0.087	0.6–1.0	+0.029	0.466
$\varphi^{(a)}$	0.031 ± 0.022	0.001–0.05	−0.009	0.177
$\varphi^{(c)}$	0.012 ± 0.011	0.005–0.05	+0.002	0.438
$\varphi^{(v)}$	0.009 ± 0.012	0.001–0.05	+0.002	0.561

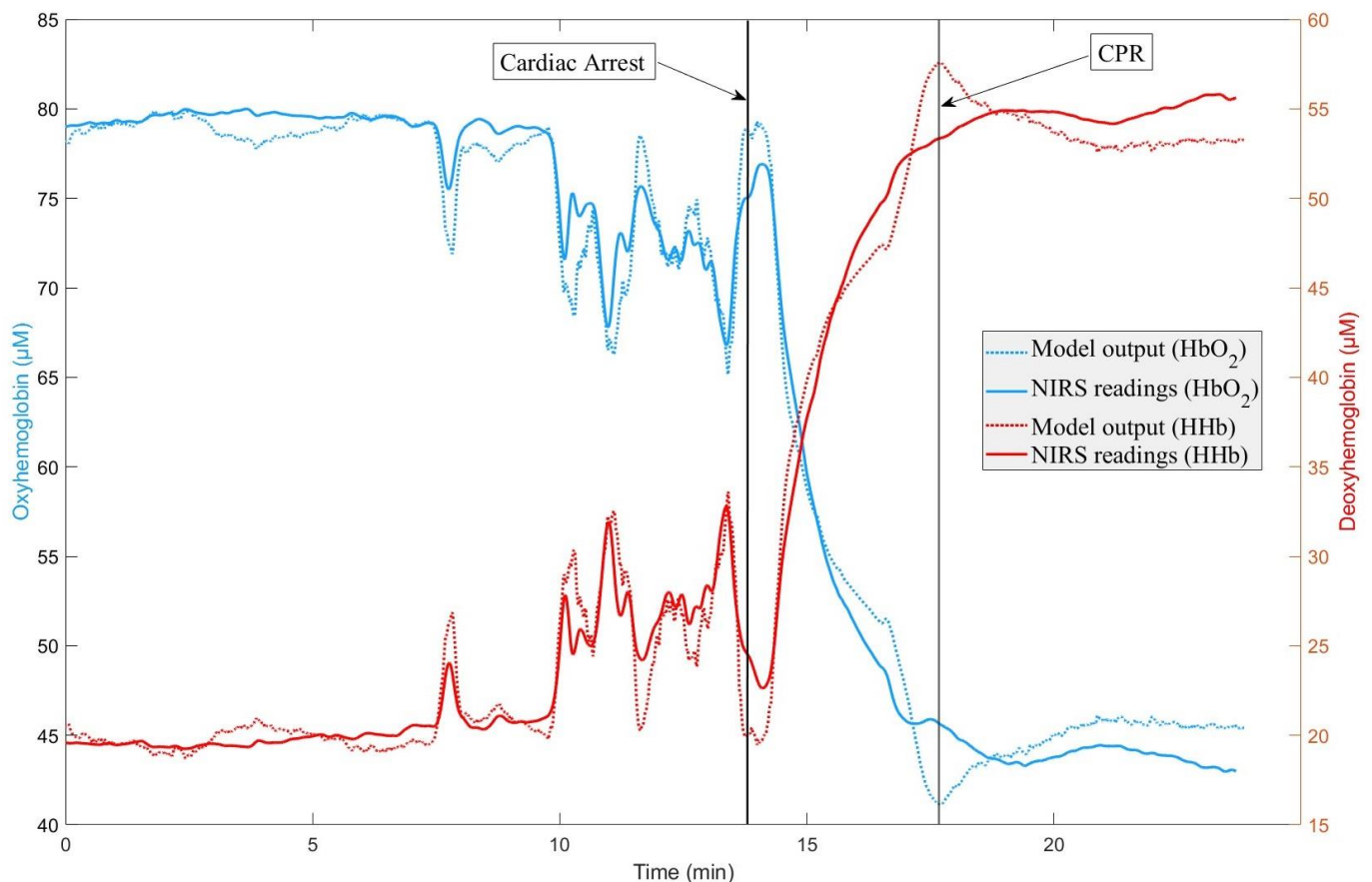


Figure 2. The solid lines (blue and red) represent NIRS readings for oxy- and deoxyhemoglobin, respectively. The dotted lines (blue and red) depict the calculated data for oxy- and deoxyhemoglobin, respectively, using the non-linear version of the model. $R^2 = 0.869$, $X^2 = 0.131$.

4. Discussion

Employing the non-linear CHS model enabled an innovative approach to the investigation of cerebral hemodynamics and metabolism during cardiac arrest and CPR, and this yielded notable insights. Using the inverse of the model, we recovered the values of the physiological parameters related to the interplay between neural activity, blood flow dynamics, and oxygenation levels.

The notable consistency between the actual near-infrared spectroscopy measurements and the model's outputs (Figure 2) underscores the accuracy with which the proposed model can capture dynamic shifts in cerebral oxygenation and blood flow. This not only validates the model, but also opens avenues for potential enhancements in resuscitation protocols which have the potential to improve outcomes for CA patients.

The reference ranges for the parameters were obtained from the literature. The mean capillary size ranged from 5.9 to 6.5 μm in diameter and from 0.57 to 0.63 μm in length [25]. The average capillary blood flow velocity was determined to be 0.85 mm/s, with a coefficient of variation equal to 0.99 [26]. The rate constant for oxygen diffusion into tissue was directly proportional to both the tissue's oxygen solubility and the microvascular partial pressure of oxygen [5]. This partial pressure depends on the metabolic rate of oxygen [27,28]. The blood volume fraction in the brain tissue can vary, with capillaries accounting for approximately 1–1.5%, and the entire microvasculature comprising about 2–4%. These values depend on the depth within the cortex [25,28]. The average baseline values we measured were all within their reference ranges. However, we note a lack of references for the rate of oxygen diffusion from blood to tissue (α_0), which was described only in the works of the group who introduced the CHS model [5,9].

We found significant differences between the baseline and post-CA values for two parameters (p -value less than 0.05 denoting meaningful distinctions). The average values for $ctHb$ and $F^{(c)}$ decreased after VF compared to the baseline. Dynamic changes in $ctHb$, both increases and decreases, had been observed previously in human CA patients [29,30]. In [29], the authors suggested that decreased $ctHb$ can be associated with worse neurological outcomes. The authors of [29,30] hypothesized that such changes may reflect the degree of vascular permeability and may be associated with neurologic function after CA. The decrease in the Fåhræus factor is most likely also related to the $ctHb$ change as it quantifies the ratio of $ctHb$ in the capillaries and larger vessels [5,9,31].

One limitation of our study became apparent following changes in HbO_2 , HHb , total hemoglobin, and CBFV which were influenced by simultaneous occurrences such as spontaneous baseline shifts, the administration of anesthesia and epinephrine, and various attempts to induce VF prior to its occurrence. The CHS model may be too simple to properly account for all such events and artifacts. This can at least partially explain why the application of the model resulted in good data fits when $R^2 > 0.5$ in only 63% of the datasets (17 out of 27). In future research, we aim to incorporate established techniques for manipulating CBF during the baseline and ROSC phases, including inducing hypercapnia, adjusting ventilation rates, and implementing similar approaches.

Another possible reason behind the differences between the model results and the readings for HHb and HbO_2 , in particular those seen in Figure 2 after the beginning of CA, is that in the current version of the CHS model, the parameters listed in Table 1 are considered to be fixed for a given time interval. However, as our analysis shows, at least $ctHb$ and $F^{(c)}$ —and possibly other parameters—can change during and after VF, leading to deviations between the real HHb and HbO_2 temporal traces and those predicted by the model with the fixed parameters. We are currently working on the further development of our dynamic model and an inversion algorithm to account for the dynamic changes in the model parameters.

Another important aspect of this study is its applicability to human studies. While there have been studies that have demonstrated significant structural and cellular compatibility between pigs and humans in various organs, such as the liver [32] and those of the cardiovascular system [33], the compatibility of the microvasculature of the brain in pigs, which was the focus of our investigation, requires more comprehensive examination. Although laser Doppler flowmetry (LDF) is an established and commercially available technique [34], it cannot measure the blood flow in the human brain non-invasively. Diffuse correlation spectroscopy (DCS) is a novel technique that measures average microvascular blood flow in tissue volumes [35]. A fast increase in the rate at which DCS is applied to brain measurements has recently started. In particular, in [36], simultaneous spatially

resolved DCS and NIRS were used to non-invasively measure cerebral microvascular parameters in humans during transient hypotension. The cerebral blood flow measurements were separated from the extracerebral contributions to the DCS signals using a combination of the short (1.5 cm) and long (2.5 cm) source-detector distances. The feasibility of using a combined hNIRS/DCS system in cardiac patients during cardiac surgery was shown in [37].

The application of the CHS model to the hNIRS data from the pig CA experiments added a practical dimension to the application of CHS, although transitioning to human parameters presents challenges. Continuing exploration and refinement of this model may lead to the elucidation of optimal CPR outcomes for the brain. This endeavor, in turn, could significantly contribute to the improvement of recovery rates following sudden CA.

Hemodynamic models can play a pivotal role in the interpretation of data from invasive and non-invasive optical imaging methods like NIRS across various microvascular hemodynamic and oxygen metabolism scenarios. This model's utility extends to scenarios involving oscillations, where utilizing the model in the frequency domain is effective. In our study of cardiac arrest in pigs, because of the singular nature of cardiac arrest and the absence of repetitive phenomena, we employed the model in the time domain.

Our investigation was initially focused on two models: the CHS model ultimately employed in our study, and another developed by a research team at the University of Essex [7]. Integrating the first model into our research marked a significant step forward. Our choice of the model employed in our study was driven by its simplicity and compatibility with our devices (hNIRS and LDF). Our interest in the latter model, which will form the basis of our future work, stems from its requirement for cytochrome c oxidase measurements—something our hNIRS device can readily provide.

The current version of our custom MATLAB code requires about 30 min of processing time per dataset on a PC with a 6-core, 3800 MHz CPU, which is slow for real-time monitoring. However, we are working on improving the algorithm, and this should result in a considerable increase in speed. After its translation into a faster programming language, the improved algorithm may enable the real-time measurement of microvascular parameters.

5. Conclusions

In this animal cardiac arrest study, we applied a CHS hemometabolic model to assess cerebral hemodynamics and metabolism during CA and CPR, with a particular focus on microvascular-level physiological changes. Our main conclusion is that the CHS hemometabolic model could explain the observed changes in 63% of cases. Notably, most of our measured parameters were in agreement with the known values; this validated our methodology and reinforced the accuracy of the results. The statistical analysis revealed significant variations between the baseline and post-VF values for the average hemoglobin concentration in the blood and the Fåhræus factor, providing insights into the impact of CA at the microvascular level.

Author Contributions: Methodology, R.M., S.L. and V.T.; Software, N.K.; Investigation, N.K. and O.R.; Data curation, R.M., N.K. and O.R.; Writing—original draft, N.K.; Writing—review & editing, R.M. and V.T.; Supervision, R.M., S.L. and V.T.; Funding acquisition, S.L. All authors have read and agreed to the published version of the manuscript.

Funding: This study was funded by a ZOLL Foundation grant. O. R. was supported by CREMS (“Comprehensive Research Experience for Medical Students”) Summer Research Program at the University of Toronto’s Temerty Faculty of Medicine.

Institutional Review Board Statement: All animals in the project will receive humane and proper treatment in accordance with the policies formulated by St. Michael’s Hospital Animal Care Committee, the Animals for Research Act 1968-69 and with the recommendations of the Canadian Council on Animal Care. PI accepts responsibility for keeping the foregoing information current especially with respect to methodology. The protocol code is 245ACC #245.

Informed Consent Statement: Not applicable.

Data Availability Statement: The results of this study are available from the corresponding author on reasonable request.

Conflicts of Interest: The authors declare no conflict of interest.

Appendix A

According to [2], changes in oxyhemoglobin resulting from changes in capillary blood flow speed and blood volume (ΔO_F and ΔO_V , respectively) (Equations (A1) and (A3), respectively) and changes in deoxyhemoglobin attributed to variations in capillary blood flow speed and blood volume (ΔD_F and ΔD_V , respectively) (Equations (A2) and (A4), respectively) are given by the following equations:

$$\Delta O_F(t) = ctHb [\varphi^{(c)} F^{(c)} (\langle S^{(c)} \rangle(t) - \langle S_0^{(c)} \rangle) + (\langle S^{(v)} \rangle(t) - S_0^{(v)})] \tag{A1}$$

$$\Delta D_F(t) = -\Delta O_F(t) \tag{A2}$$

$$\Delta O_v(t) = ctHb [\varphi^{(a)} S^{(a)} v^{(a)}(t) + \varphi^{(a)} \langle S^{(v)} \rangle(t) v^{(v)}(t)] \tag{A3}$$

$$\Delta D_v(t) = ctHb [\varphi^{(a)} (1 - S^{(a)}) v^{(a)}(t) + \varphi^{(a)} (1 - \langle S^{(v)} \rangle(t)) v^{(v)}(t)] \tag{A4}$$

where $ctHb$ represents hemoglobin concentration in the blood, $\varphi^{(c)}$ and $\varphi^{(a)}$ denote the volume fractions of capillary and arterial blood in the tissue, respectively, $F^{(c)}$ stands for the Fåhræus factor, $\langle S^{(c)} \rangle(t)$ indicates the average capillary saturation, $v^{(a)}$ and $v^{(v)}$ signify the changes in arterial and venous blood volumes normalized to their baseline values, $S^{(a)}$ represents arterial saturation, and $\langle S^{(v)} \rangle(t)$ represents the venule saturation. The capillary and venule oxygen saturations can be calculated using the following equations [2]:

$$c^{(c)}(t) \frac{\partial S^{(c)}(x, t)}{\partial x} + \frac{\partial S^{(c)}(x, t)}{\partial t} = -\alpha_o S^{(c)}(x, t) \tag{A5}$$

$$c^{(v)}(t) \frac{\partial S^{(v)}(x, t)}{\partial x} + \frac{\partial S^{(v)}(x, t)}{\partial t} = 0 \tag{A6}$$

References

1. Yan, S.; Gan, Y.; Jiang, N.; Wang, R.; Chen, Y.; Luo, Z.; Zong, Q.; Chen, S.; Lv, C. The global survival rate among adult out-of-hospital cardiac arrest patients who received cardiopulmonary resuscitation: A systematic review and meta-analysis. *Crit. Care* **2020**, *24*, 61. [CrossRef] [PubMed]
2. Smith, M. Shedding light on the adult brain: A review of the clinical applications of near-infrared spectroscopy. *Philos. Trans. R. Soc. A Math. Phys. Eng. Sci.* **2011**, *369*, 4452–4469. [CrossRef] [PubMed]
3. Kolyva, C.; Ghosh, A.; Tachtsidis, I.; Highton, D.; Cooper, C.E.; Smith, M.; Elwell, C.E. Cytochrome c oxidase response to changes in cerebral oxygen delivery in the adult brain shows higher brain-specificity than haemoglobin. *NeuroImage* **2014**, *85 Pt 1*, 234–244. [CrossRef]
4. Hashem, M.; Zhang, Q.; Wu, Y.; Johnson, T.W.; Dunn, J.F. Using a multimodal near-infrared spectroscopy and MRI to quantify gray matter metabolic rate for oxygen: A hypothermia validation study. *NeuroImage* **2020**, *206*, 116315. [CrossRef] [PubMed]
5. Sassaroli, A.; Kainerstorfer, J.M.; Fantini, S. Nonlinear extension of a hemodynamic linear model for coherent hemodynamics spectroscopy. *J. Theor. Biol.* **2016**, *389*, 132–145. [CrossRef]
6. Hiura, M.; Funaki, A.; Shibusaki, H.; Takahashi, K.; Katayama, Y. Dissociated coupling between cerebral oxygen metabolism and perfusion in the prefrontal cortex during exercise: A NIRS study. *Front. Physiol.* **2023**, *14*, 1165939. [CrossRef]
7. Blaney, G.; Fernandez, C.; Sassaroli, A.; Fantini, S. Dual-slope imaging of cerebral hemodynamics with frequency-domain near-infrared spectroscopy. *Neurophotonics* **2023**, *10*, 013508. [CrossRef]
8. Blaney, G.; Sassaroli, A.; Fantini, S. Algorithm for determination of thresholds of significant coherence in time-frequency analysis. *Biomed. Signal Process. Control* **2020**, *56*, 101704. [CrossRef]

9. Fantini, S. Dynamic model for the tissue concentration and oxygen saturation of hemoglobin in relation to blood volume, flow velocity, and oxygen consumption: Implications for functional neuroimaging and coherent hemodynamics spectroscopy (CHS). *NeuroImage* **2014**, *85 Pt 1*, 202–221. [[CrossRef](#)]
10. Banaji, M.; Mallet, A.; Elwell, C.E.; Nicholls, P.; Cooper, C.E. A Model of Brain Circulation and Metabolism: NIRS Signal Changes during Physiological Challenges. *PLoS Comput. Biol.* **2008**, *4*, e1000212. [[CrossRef](#)]
11. Russell-Buckland, J.; Tachtsidis, I. Developing a Model to Simulate the Effect of Hypothermia on Cerebral Blood Flow and Metabolism. *Adv. Exp. Med. Biol.* **2020**, *1232*, 299–306. [[CrossRef](#)]
12. Russell-Buckland, J.; Barnes, C.P.; Tachtsidis, I. A Bayesian framework for the analysis of systems biology models of the brain. *PLoS Comput. Biol.* **2019**, *15*, e1006631. [[CrossRef](#)] [[PubMed](#)]
13. Siddiqui, M.F.; Lloyd-Fox, S.; Kaynezhad, P.; Tachtsidis, I.; Johnson, M.H.; Elwell, C.E. Non-invasive measurement of a metabolic marker of infant brain function. *Sci. Rep.* **2017**, *7*, 1330. [[CrossRef](#)] [[PubMed](#)]
14. Caldwell, M.; Scholkmann, F.; Wolf, U.; Wolf, M.; Elwell, C.; Tachtsidis, I. Modelling confounding effects from extracerebral contamination and systemic factors on functional near-infrared spectroscopy. *NeuroImage* **2016**, *143*, 91–105. [[CrossRef](#)]
15. Hapuarachchi, T.; Scholkmann, F.; Caldwell, M.; Hagmann, C.; Kleiser, S.; Metz, A.J.; Pastewski, M.; Wolf, M.; Tachtsidis, I. Simulation of Preterm Neonatal Brain Metabolism During Functional Neuronal Activation Using a Computational Model. *Adv. Exp. Med. Biol.* **2016**, *876*, 111–120, E1–E2. [[CrossRef](#)]
16. Caldwell, M.; Moroz, T.; Hapuarachchi, T.; Bainbridge, A.; Robertson, N.J.; Cooper, C.E.; Tachtsidis, I. Modelling Blood Flow and Metabolism in the Preclinical Neonatal Brain during and Following Hypoxic-Ischaemia. *PLoS ONE* **2015**, *10*, e0140171. [[CrossRef](#)] [[PubMed](#)]
17. Nosrati, R.; Lin, S.; Mohindra, R.; Ramadeen, A.; Toronov, V.; Dorian, P. Study of the Effects of Epinephrine on Cerebral Oxygenation and Metabolism During Cardiac Arrest and Resuscitation by Hyperspectral Near-Infrared Spectroscopy. *Crit. Care Med.* **2019**, *47*, e349–e357. [[CrossRef](#)]
18. McAnally, J.R. The use of animals in research . . . the views of a young researcher. *J. Okla. Dent. Assoc.* **1993**, *83*, 34–35.
19. Nosrati, R.; Lin, S.; Ramadeen, A.; Monjazebi, D.; Dorian, P.; Toronov, V. Cerebral Hemodynamics and Metabolism During Cardiac Arrest and Cardiopulmonary Resuscitation Using Hyperspectral Near Infrared Spectroscopy. *Circ. J.* **2017**, *81*, 879–887. [[CrossRef](#)]
20. Nosrati, R.; Ramadeen, A.; Hu, X.; Woldemichael, E.; Kim, S.; Dorian, P.; Toronov, V. Simultaneous measurement of cerebral and muscle tissue vc during cardiac arrest and cardiopulmonary resuscitation. In *Optical Techniques in Neurosurgery, Neurophotonics, and Optogenetics II*; SPIE: Bellingham, WA, USA, 2015; Volume 9305, pp. 164–169.
21. Zhao, H.; Tanikawa, Y.; Gao, F.; Onodera, Y.; Sassaroli, A.; Tanaka, K.; Yamada, Y. Maps of optical differential pathlength factor of human adult forehead, somatosensory motor and occipital regions at multi-wavelengths in NIR. *Phys. Med. Biol.* **2002**, *47*, 2075–2093. [[CrossRef](#)]
22. Strangman, G.E.; Li, Z.; Zhang, Q. Depth Sensitivity and Source-Detector Separations for Near Infrared Spectroscopy Based on the Colin27 Brain Template. *PLoS ONE* **2013**, *8*, e66319. [[CrossRef](#)] [[PubMed](#)]
23. Scholkmann, F.; Wolf, M. General equation for the differential pathlength factor of the frontal human head depending on wavelength and age. *J. Biomed. Opt.* **2013**, *18*, 105004. [[CrossRef](#)] [[PubMed](#)]
24. Yeganeh, H.Z.; Toronov, V.; Elliott, J.T.; Diop, M.; Lee, T.-Y.; Lawrence, K.S. Broadband continuous-wave technique to measure baseline values and changes in the tissue chromophore concentrations. *Biomed. Opt. Express* **2012**, *3*, 2761–2770. [[CrossRef](#)] [[PubMed](#)]
25. Cassot, F.; Lauwers, F.; Fouard, C.; Prohaska, S.; Lauwers-Cances, V. A Novel Three-Dimensional Computer-Assisted Method for a Quantitative Study of Microvascular Networks of the Human Cerebral Cortex. *Microcirculation* **2006**, *13*, 1–18. [[CrossRef](#)]
26. Pries, A.R.; Secomb, T.W.; Gaehtgens, P. Structure and hemodynamics of microvascular networks: Heterogeneity and correlations. *Am. J. Physiol.* **1995**, *269 Pt 2*, H1713–H1722. [[CrossRef](#)]
27. Secomb, T.W.; Hsu, R.; Dewhirst, M.W.; Klitzman, B.; Gross, J.F. Analysis of oxygen transport to tumor tissue by microvascular networks. *Int. J. Radiat. Oncol. Biol. Phys.* **1993**, *25*, 481–489. [[CrossRef](#)]
28. Zheng, Y.; Martindale, J.; Johnston, D.; Jones, M.; Berwick, J.; Mayhew, J. A Model of the Hemodynamic Response and Oxygen Delivery to Brain. *NeuroImage* **2002**, *16 Pt 1*, 617–637. [[CrossRef](#)]
29. Albaeni, A.; Eid, S.M.; Akinyele, B.; Kurup, L.N.; Vaidya, D.; Chandra-Strobos, N. The association between post resuscitation hemoglobin level and survival with good neurological outcome following out of hospital cardiac arrest. *Resuscitation* **2016**, *99*, 7–12. [[CrossRef](#)]
30. Schrieffl, C.; Schoergenhofer, C.; Ettl, F.; Poppe, M.; Clodi, C.; Mueller, M.; Grafeneder, J.; Jilma, B.; Magnet, I.A.M.; Buchtele, N.; et al. Change of Hemoglobin Levels in the Early Post-cardiac Arrest Phase Is Associated With Outcome. *Front. Med.* **2021**, *8*, 639803. [[CrossRef](#)]
31. Liang, Z.; Tian, H.; Yang, H.-C.S.; Arimitsu, T.; Takahashi, T.; Sassaroli, A.; Fantini, S.; Niu, H.; Minagawa, Y.; Tong, Y. Tracking Brain Development From Neonates to the Elderly by Hemoglobin Phase Measurement Using Functional Near-Infrared Spectroscopy. *IEEE J. Biomed. Health Inform.* **2021**, *25*, 2497–2509. [[CrossRef](#)]
32. Ntonas, A.; Katsourakis, A.; Galanis, N.; Filo, E.; Noussios, G. Comparative Anatomical Study Between the Human and Swine Liver and Its Importance in Xenotransplantation. *Cureus* **2020**, *12*, e9411. [[CrossRef](#)] [[PubMed](#)]

33. Lelovas, P.P.; Kostomitsopoulos, N.G.; Xanthos, T.T. A comparative anatomic and physiologic overview of the porcine heart. *J. Am. Assoc. Lab. Anim. Sci.* **2014**, *53*, 432–438. [[PubMed](#)]
34. Bottino, D.A.; Bouskela, E. Non-invasive techniques to access in vivo the skin microcirculation in patients. *Front. Med.* **2023**, *9*, 1099107. [[CrossRef](#)] [[PubMed](#)]
35. Boas, D.A.; Sakadžić, S.; Selb, J.; Farzam, P.; Franceschini, M.A.; Carp, S.A. Establishing the diffuse correlation spectroscopy signal relationship with blood flow. *Neurophotonics* **2016**, *3*, 031412. [[CrossRef](#)]
36. Shoemaker, L.N.; Milej, D.; Mistry, J.; Lawrence, K.S. Using depth-enhanced diffuse correlation spectroscopy and near-infrared spectroscopy to isolate cerebral hemodynamics during transient hypotension. *Neurophotonics* **2023**, *10*, 025013. [[CrossRef](#)]
37. Rajaram, A.; Milej, D.; Suwalski, M.; Yip, L.C.M.; Guo, L.R.; Chu, M.W.A.; Chui, J.; Diop, M.; Murkin, J.M.; Lawrence, K.S. Optical monitoring of cerebral perfusion and metabolism in adults during cardiac surgery with cardiopulmonary bypass. *Biomed. Opt. Express* **2020**, *11*, 5967–5981. [[CrossRef](#)]

Disclaimer/Publisher’s Note: The statements, opinions and data contained in all publications are solely those of the individual author(s) and contributor(s) and not of MDPI and/or the editor(s). MDPI and/or the editor(s) disclaim responsibility for any injury to people or property resulting from any ideas, methods, instructions or products referred to in the content.